Quantification of anionic redox chemistry in a prototype Na-rich layered oxide

Yue Hu,[1+] Tiefeng Liu,[2+] Chen Cheng,[1] Yingying Yan,[1] Manling Ding,[1] Ting-Shan Chan,[3] Jinghua Guo,[4,5] and Liang Zhang[1*]

1. Institute of Functional Nano & Soft Materials (FUNSOM), Jiangsu Key Laboratory for Carbon-Based Functional Materials & Devices, Soochow University, 199 Ren'ai Road, Suzhou 215123, Jiangsu, China

2. College of Materials Science and Engineering, Zhejiang University of Technology, Hangzhou 310014, Zhejiang, China

3. National Synchrotron Radiation Research Center, Hsinchu 30076, Taiwan

4. Advanced Light Source, Lawrence Berkeley National Laboratory, Berkeley, California 94720, USA

5. Department of Chemistry and Biochemistry, University of California, Santa Cruz, California 95064, USA

[+]These two authors contributed equally to this work.

*Email: liangzhang2019@suda.edu.cn

Abstract

Harnessing anionic redox reactions is of prime importance for boosting the capacity of sodium-ion batteries. However, quantifying the cyclability of anionic redox reactions is still challenging. Herein, we conduct a qualitative and quantitative investigation of the cationic and anionic redox reactions of a prototype Na-rich layered oxide, namely Na_3RuO_4, by a combination of bulk-sensitive X-ray absorption spectroscopy (XAS) and full-range mapping of resonant inelastic X-ray scattering

(mRIXS). We unequivocally reveal that both Ru cations and oxygen anions are involved in the charge compensation process of Na_3RuO_4. The Ru redox is highly reversible over extended electrochemical cycles; while the cyclability of lattice oxygen redox gradually decreases with the retention of only 36% after 30 cycles, which is mainly responsible for the capacity fading of Na_3RuO_4. Our findings provide deeper insights into the complex oxygen redox mechanism, which plays a decisive role for designing high-energy Na-rich electrode materials for sodium-ion batteries.

1. Introduction

Electrochemical energy storage is one of the most convenient and cost-effective energy storage methods.[1-2] Among miscellaneous advanced energy storage devices, lithium-ion batteries (LIBs) are indispensable in our daily lives by enabling portable electronic and EV markets. However, the expected increase of the raw lithium cost has led to the search of cost–effectiveness alternative batterie. Sodium-ion batteries (SIBs) are considered as promising candidates for next generation batteries due to the similar ion storage mechanism and the abundant low-cost sodium resources.[3-5] For SIBs, the cathode materials play a vital role for determining the overall performance, e.g., power density, energy density, and lifetime. A broad range of compounds, such as layered oxides, Prussian blue analogues, and polyanionic compounds, have been extensively investigated as the possible cathode materials for SIBs.[6-11] Nevertheless, there are still some concerns regarding the limited energy density and structural instability of these electrodes over extended cycling.[12-15] As a consequence, it is highly required to develop new electrode materials for SIBs with high energy density and long lifetime.

The recent discovery of Li-rich layered oxide electrodes with the involvement of both cationic and anionic redox activities opens up a feasible direction to boost the cathode capacity.[16-19] Inspired by this paradigm, great efforts have also been devoted to introducing anionic redox activity into Na-ion electrodes.[20-21] Most recently, Na_3RuO_4 was introduced as a pure prototype Na-rich layered oxide for SIBs, which delivers an outstanding electrochemical performance.[22-23] However, the charge compensation mechanism of Na_3RuO_4 undergoes different hypotheses: (i) Qiao *et al.* proposed that during the charge and discharge processes Ru cations are inert and merely oxygen anions contribute to the reversible capacity,[22] and (ii) Otoyama *et al.* believed that both Ru and

oxygen are involved into the charge compensation process with Ru^{6+} and peroxo-like species as the oxidation products during the first few charge cycles.[23] It is clear that the understanding of the cationic and anionic redox reactions of Na_3RuO_4 is still limited, mainly because (i) there is still no consensus on whether Ru cations are electrochemically active or not; (ii) the charge compensation mechanism was investigated merely for the first cycle without quantification; and (iii) more importantly, despite prevailing O-K spectroscopies, particularly X-ray absorption spectroscopy (XPS) and X-ray absorption spectroscopy (XAS), have been popularly applied to investigate the anionic redox reaction mechanism, direct and reliable evidence for validating the participation of intrinsic oxygen redox process is still rarely reported due to the shallow probe depth of XPS and intricate TM-O hybrid effect in XAS.[24-25]

In this work, we have investigated the cationic and anionic redox mechanism of Na_3RuO_4 over extended electrochemical cycles by using bulk-sensitive XAS and full-range mapping of resonant inelastic X-ray scattering (mRIXS) techniques. The combination of XAS and mRIXS offers quantitative analysis and unprecedented insights into intrinsic oxygen redox mechanism for Na-rich electrode materials. Here, we provide robust evidence that both Ru and O are involved in the redox process. While the Ru redox is highly reversible during the cycling process, the lattice oxygen redox cyclability continues decreasing with the capacity retention of only 36% after 30 cycles, which should be responsible for the gradual capacity fading of Na_3RuO_4 electrode. We believe that these findings should have important implications for the further design and optimization of Na-rich electrodes with anionic redox for SIBs.

2. Results and discussion

Na_3RuO_4 was prepared by a conventional solid-state reaction and characterized by powder X-ray

diffraction (XRD) (Figure 1a). The XRD patterns are very similar to those reported in the literature, suggesting the successful synthesis of high-purity Na_3RuO_4.[22-23] As summarized previously, Na_3RuO_4 adopts a Na-rich layered structure where the stacking of alternating Na^+ and $(Na_{1/2}Ru_{1/2})O_2^-$ layers along the c-axis, and the isolated tetramers of edge-sharing RuO_6 octahedra was separated by sodium atoms in the $(Na_{1/2}Ru_{1/2})O_2^-$ layer.[22-23] The SEM images of Na_3RuO_4 (Figure 1b and c) show nonuniform nanometer-sized particles induced by the solid-state reaction process. In addition, the corresponding energy dispersive spectra (EDS) results clearly demonstrate that Ru, Na and O atoms are uniformly distributed throughout the sample (Figure 1d−g). Overall, the above results indicate that Na_3RuO_4 with well-defined crystal structure has been successfully synthesized.
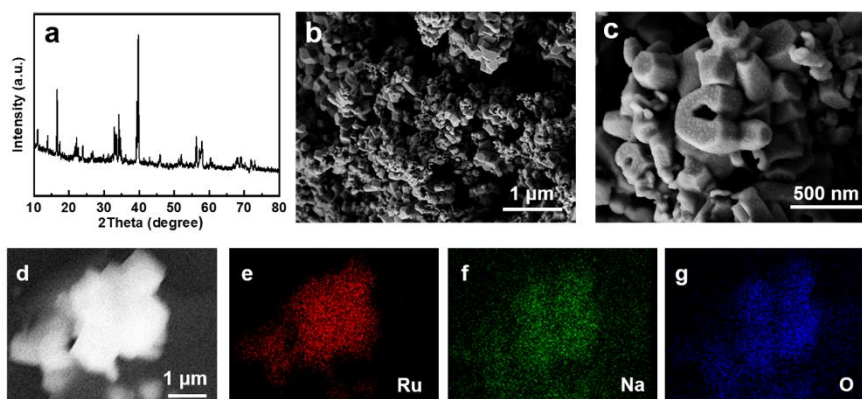

Figure 1. Structure characterization of as-prepared Na_3RuO_4 nanoparticles. (a) XRD pattern. (b-c) SEM images. (d–e) EDS of Na_3RuO_4, showing the homogeneous distribution of Ru, Na, and O elements.

The electrochemical performance of Na_3RuO_4 electrode was then evaluated through galvanostatic charge/discharge process between 1.5 and 4.0 V using 1M $NaClO_4$ in EC/PC (1/1 wt) as the electrolyte, as shown in Figure S1. An initial capacity of 115 mAh/g was delivered upon charging, which corresponds to ~0.97 Na per formula unit. Despite suffering from a large irreversible capacity,

partial Na ions can still be re-intercalated back to the host with a discharge capacity of 92 mAh/g. The irreversible capacity could be related to the inevitable electrolyte decomposition and/or irreversible oxygen release, as will be discussed in detail later.

To grasp deeper insight into the charge compensation mechanism of Na_3RuO_4 upon Na ions extraction and insertion, we conducted XAS measurements using bulk-sensitive total fluorescence yield (TFY) mode on Na_3RuO_4 electrodes cycled to different states of charge (SOC) (Figure 2c). We first recorded Ru L-edge XAS to clarify the oxidation state evolution of Ru as a function of SOC. The advantage of Ru L-edge XAS is that it can directly detect the unoccupied 4d states through dipole-allowed 2p-4d transitions, which are the key evolving electronic states for Ru-based electrode materials.[11, 26] Figure 2a shows the corresponding XAS results of Na_3RuO_4 at different SOC of the first cycle. For the spectrum of pristine Na_3RuO_4 $(t_{2g}^3 e_g^0)$, it contains two deconvoluted peaks located at 2839.1 and 2841.5 eV, corresponding to $2p \rightarrow t_{2g}$ and $2p \rightarrow e_g$ transitions, respectively.[27-28] The peak position matches well with that of Ru^{5+} in an ordered double perovskite $SrY_{1/2}Ru_{1/2}O_3$,[29] confirming that ruthenium mainly has a +5 oxidation state in pristine Na_3RuO_4. Interestingly, the absorption peak shifts gradually toward higher energy upon the whole charge process, which indicates the continuous increase of the oxidation state of Ru. Although it is technically difficult to identify the exact final oxidation state of Ru, we believe that Ru cannot be oxidized to +6 as deduced from previous reported energy/oxidation state calibration.[27] On the other hand, the initial charge capacity is 115.7 mAh/g, which is lower than the theoretical value of 118.8 mAh/g (assuming 1.0-electron reaction). Therefore, it is rational to assume that the Ru oxidation state should be between +5 and +6. During the subsequent discharge process, the absorption peak gradually shifts back to the initial position, indicating the reversible redox reaction of Ru during the

initial cycle. It should be noted that the different capacity reported here compared with that of previous studies may be related to the cation ordering of Na-rich materials, as revealed for ordered Na_2RuO_3 and honeycomb-ordered Na_2RuO_3.[27] Nonetheless, this should not influence the electrochemical activity of Ru.
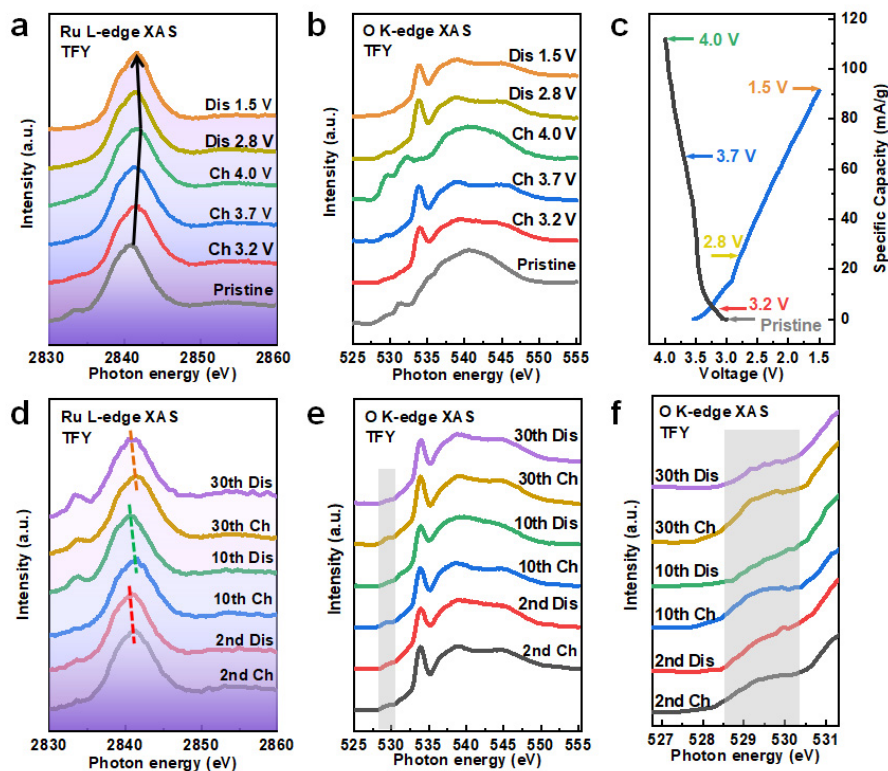

Figure 2. XAS of Na_3RuO_4 electrodes cycled in the voltage range of 1.5-4.0 V. (a) Ru L_3-edge XAS at different SOC of the initial cycle. (b) O K-edge XAS at different SOC of the initial cycle. (c) Charge/discharge voltage profiles of the initial cycle. The points measured by XAS and mRIXS are marked with arrows. (d) Ru L_3-edge XAS after different cycles. (e) O K-edge XAS after different cycles. (f) Enlarged view of the pre-edge area of O K-edge XAS shown in Figure (e).

To further investigate whether Ru cations remain active over extended cycles, we next measured Ru L-edge XAS of Na_3RuO_4 upon extended cycles, as shown in Figure 2d. It is clear that the main absorption feature shifts toward higher energy and shift back to lower energy as Na ions are

extracted and inserted, respectively, indicating that Ru cations are oxidized upon charge and reduced upon discharge. Accompanied with the fact that the energy shifts are similar for different electrochemical cycles, these results strongly indicate the high reversibility of Ru redox reaction upon extended cycling.

This scenario is also verified by the corresponding O K-edge XAS spectra. As discussed in previous reports, the spectral shape change of O K-edge XAS does not represent oxygen redox but provides indirect evidence for transition metal (TM) redox.[24, 30] Figure 2b shows the O K-edge XAS spectra of Na₃RuO₄ electrodes cycled to different SOC. For the spectrum of pristine Na₃RuO₄, the pre-edge features around 529.5 eV and 531.5 eV correspond to the unoccupied O 2p-Ru t_{2g} and O 2p-Ru e_g states, respectively, while the broad peak at 534.5 eV is related to the O 2p-Ru 5sp hybridization state.[27, 31-34] The evolution of pre-edge region in O K-edge XAS spectra reflects the oxidation state change of Ru. With the charge of Na₃RuO₄ electrode, electrons are extracted from the system through the desodiation process, resulting in the enhancement of the pre-edge region and thus the oxidation state of Ru. This observation is consistent with the evolution of Ru L-edge XAS. Of note, a significant feature located at 534 eV, which corresponds to the π* feature of carbonate (CO_3^{2-}), is formed during the cycling process. The formation of carbonate species could originate from the degradation of electrolyte at the electrode-electrolyte interface, which has also been frequently observed for other electrode materials for SIBs.[27, 35-37] Interestingly, the spectral shape of Na₃RuO₄ electrode charged to 4.5 V is quite different from that of the remaining spectra, which may be related to the oxygen release from the electrode after charging to high voltage,[34, 37] especially for the initial cycle. The high reversibility of Ru redox over prolonged cycles is also verified by O K-edge XAS of Na₃RuO₄ after different cycles, as shown in Figure 2e and f, which clearly

demonstrates the enhancement and suppression of pre-edge feature during the charge and discharge processes, respectively. Therefore, the capacity fading of Na_3RuO_4 should be not related to cation redox but most likely related to anion redox, as will be discussed in detail in the following section.
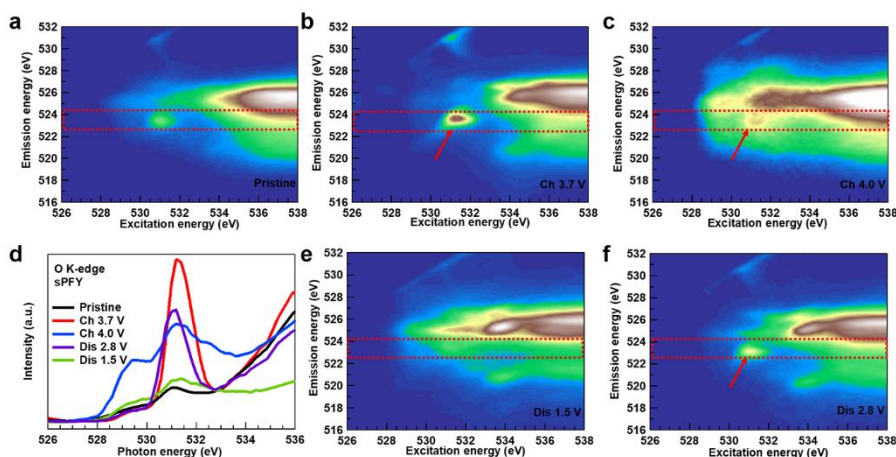

Figure 3. O-K mRIXS and sPFY of Na_3RuO_4 electrodes of the first cycle. (a-c) The mRIXS images at different SOCs during the charge process. The red arrows represent the key oxygen redox characteristics at electrochemical processes. (d) sPFY spectra extracted from mRIXS by integrating the signals around the characteristic 523.7 eV emission energy range, as marked by the red dashed box. (e-f) The mRIXS images of Na_3RuO_4 electrodes at different SOCs during the discharge process.

As an effective probe of the intrinsic lattice oxygen activity, mRIXS has been applied to investigate the oxygen redox reaction of electrode materials for both SIBs and LIBs.[25, 38-39] The advantage of mRIXS compared with XAS is that it can provide new dimensional information on emission energy.[40-41] For instance, the specific RIXS feature emerged at 523.7 eV emission and 531.0 eV excitation energies for charged electrode materials distinguishes the oxidized oxygen that is involved in the oxygen redox reaction from that of TM-O hybridization feature located at 525 eV emission energy.[24, 38-39] Hence, mRIXS can decipher the diverse oxygen states concealed in the pre-edge region of O-K XAS.

Figure 3 shows the O K-edge mRIXS of Na_3RuO_4 electrodes obtained throughout the first cycle along with the super-partial fluorescence yield (sPFY) in **Figure 3d**. The mRIXS results are plotted against the excitation energy (*x* axis) and emission energy (*y* axis). For the pristine Na_3RuO_4 electrode, the weak but discernable emission features with the excitation energies of 528-532 eV correspond to the Ru 4d-O 2p hybridization states, while the broad emission features above 535 eV excitation energies are related to the Ru 5sp-O 2p hybridization states. Interestingly, for Na_3RuO_4 charged to 3.7 V, a striking RIXS feature at excitation and emission energies of 531.0 eV and 523.7 eV (marked by red arrow in Figure 3b) appears, and during the following discharge this feature gradually gets weakened and almost disappears after discharge to 1.5 V. This observation clearly implies the involvement of reversible lattice oxygen redox reaction for Na_3RuO_4.[25] This conclusion is further verified by sPFY spectra at different SOC of Na_3RuO_4 (Figure 3d). The advantage of sPFY is that it displays the distinct lattice oxygen redox feature, in contrast to the conventional XAS dominated by TM-O hybridization states and other oxygen-related species (e.g., CO_3^{2-} shown in Figure 2b and e). The sPFY spectra apparently demonstrate the increase and decrease of the characteristic oxidized oxygen feature at ~531 eV during the charge and discharge processes, respectively, highlighting the involvement and reversibility of the lattice oxygen redox reaction. Interestingly, this fingerprint feature shows a noticeable decrease when charging from 3.7 V to 4.0 V. This abnormal behavior may be related to the O_2 release at high charge voltage, which has been frequently observed for electrode materials of LIBs and SIBs.[34, 37-38] The release of O_2 is possibly accompanied by the migration of metal cations and creation of structural disorder,[18, 42] leading to the decrease of oxidized oxygen feature and change of total spectral shape.

The presence of reversible lattice oxygen redox for Na_3RuO_4 is likely to be correlated to the

following factors: (1) the optimal Na/Ru ratio in Na_3RuO_4. Recent studies disclosed that the local atomic coordination around oxygen atoms in layered oxides could be affected via increasing the Na (Li) content, which can improve the lattice oxygen redox upon electrochemical cycling.[21, 43-45] Therefore, it is reasonable to assume that the high Na/Ru ratio in Na-rich layered oxide Na_3RuO_4 could facilitate the oxygen redox process. (2) The highly covalent nature of Ru 4d-O 2p hybridization orbitals. Compared to previously reported oxygen redox in 3d-based Na/Li-rich layered oxides, oxygen redox appears to be boosted in the 4d/5d-based Na/Li-rich layered oxide.[21, 46-48] In contrast to the relatively weak TM 3d-O 2p covalent bond, the strong TM 4d/5d-O 2p covalent bond is beneficial for the reversible oxygen redox process, which can effectively suppress the oxygen gas release.[26] Consequently, the highly-covalent Ru-O bond should also be responsible for the reversible oxygen redox reaction of Na_3RuO_4.
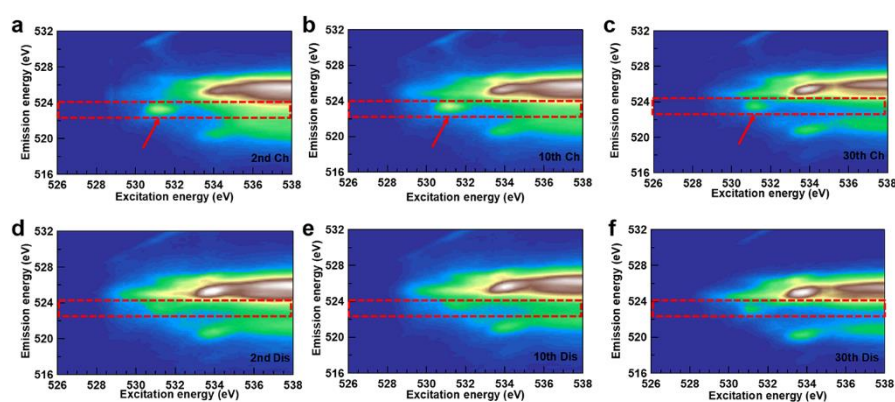

Figure 4. O-K mRIXS of Na_3RuO_4 over extended cycles. (a) 2nd charge. (b) 10th charge. (c) 30th charge. (d) 2nd discharge. (e) 10th discharge. (f) 30th discharge.

To further quantify the cyclability of oxygen redox, which is still rarely assessed for Na-rich electrode materials, we measured O K-edge mRIXS of Na_3RuO_4 upon extended electrochemical cycles by use of the characteristic oxygen redox feature in mRIXS and the quantitative analysis of oxygen redox peak in sPFY. As shown in Figure 4, the oxygen redox feature shows a decent

cyclability over 30 cycles, with an emergence at charged state (red arrows in top row) and disappearance at discharged state (bottom row). The quantification of oxygen redox cyclability is realized from sPFY results by integrating the same energy window shown in Figure 3d. The intensity of the 531 eV peak varies significantly under different electrochemical conditions, as shown in Figure 5a. We quantify the amounts of oxygen redox at different cycles by the intensity difference of the sPFY 531-eV peak area between fully charged and discharged states for the 2nd, 10th and 30th cycles (denoted as a_i, i represents the cycle number), and the cyclability is calculated by a_i/a_1, as shown in Figure 5b.[25] The data show that the oxygen redox cyclability is 76.3%, 72.9%, and 36.1%, for the 2nd, 10th, and 30th cycles, respectively. These results explicitly suggest that the oxygen redox cyclability decreases gradually with the increase of cycle number, which should be the main reason for the continuous capacity fading of Na_3RuO_4 electrodes.
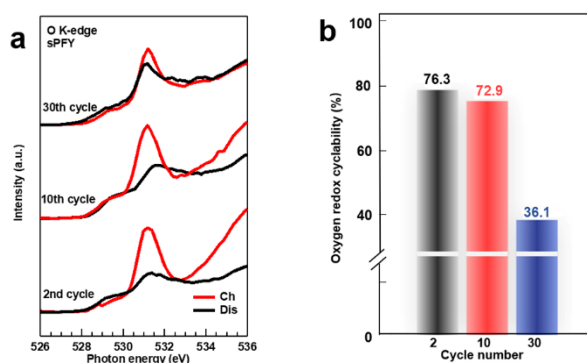

Figure 5. (a) O-K sPFY of Na_3RuO_4 over extended cycles, as derived from Figure 4 by integrating the mRIXS area around 523.7 eV emission energy. (b) Quantification of the oxygen redox cyclability derived from Figure 5a.

There are several possibilities for the decrease of oxygen redox cyclability over cycling. It has been found that there exists a continuous lattice distortion in Na-excess layered materials during the sodiation-desodiation processes, which can lead to the irreversible phase transition, the emergence of primary grain cracks, and therefore the less oxygen redox cyclability and capacity fading.[49-50] In

addition, the formation and accumulation of electrolyte decomposition compounds (e.g., carbonate species) at the electrode surface possibly makes the oxygen redox reaction kinetically sluggish, which can further affect the cyclability of the oxygen redox.[13]

3. Conclusions

In summary, we have thoroughly investigated the charge compensation mechanism of Na_3RuO_4 qualitatively and quantitatively by a combination of XAS and mRIXS. We reveal that Ru cations also participate in the charge compensation mechanism of Na_3RuO_4 with a high reversibility over prolonged cycles, clarifying the previous debate about the electrochemical activity of Ru in Na_3RuO_4. In addition, we directly prove that the oxygen redox process remains over extended cycling by the virtue of mRIXS. The highly-covalent Ru-O bond and the optimal Na/Ru ratio in Na_3RuO_4 are likely to be responsible for the observed reversible lattice oxygen redox behavior. More importantly, we provide a solid evidence that the lattice oxygen redox cyclability continues decreasing with the retention of only 36% after 30 cycles, which is the main reason for the capacity fading of Na_3RuO_4. We believe this study is of great significance for deeper understanding and assessing the cation and anion redox of prototype Na-rich layered oxide Na_3RuO_4, which should be beneficial for the further development of high-performance Na-rich electrodes for SIBs.

References

1.   Hu, L.; Cui, Y., Energy and environmental nanotechnology in conductive paper and textiles. *Energy Environ. Sci.* **2012**, *5*, 6423.

2.   Meng, X.; Yang, X. Q.; Sun, X., Emerging Applications of Atomic Layer Deposition for Lithium-Ion Battery Studies. *Adv. Mater.* **2012**, *24*, 3589-615.

3.   Song, S.; Kotobuki, M.; Zheng, F.; Xu, C.; Savilov, S. V.; Hu, N.; Lu, L.; Wang, Y.; Li, W. D. Z., A hybrid polymer/oxide/ionic-liquid solid electrolyte for Na-metal batteries. *J. Mater. Chem. A* **2017**, *5*, 6424-6431.

4.   Armand, M.; J-M, T., Building better batteries. *Nature* **2008**, *451*, 652-657.

5.   Liu, T.; Zhang, Y.; Jiang, Z.; Zeng, X.; Ji, J.; Li, Z.; Gao, X.; Sun, M.; Lin, Z.; Ling, M.; Zheng, J.; Liang, C., Exploring competitive features of stationary sodium ion batteries for electrochemical energy storage. *Energy Environ. Sci.* **2019**, *12*, 1512-1533.

6.   Abraham, K. M., Prospects and Limits of Energy Storage in Batteries. *J. Phys. Chem. Lett.* **2015**, *6*, 830-844.

7.   Lu, Y.; Wang, L.; Cheng, J.; Goodenough, J. B., Prussian blue: a new framework of electrode materials for sodium batteries. *Chem. Commun.* **2012**, *48*, 6544-6546.

8.   You, Y.; Wu, X.-L.; Yin, Y.-X.; Guo, Y.-G., High-quality Prussian blue crystals as superior cathode materials for room-temperature sodium-ion batteries. *Energy Environ. Sci.* **2014**, *7* (5),

1643-1647.

9. Gong, Z.; Yang, Y., Recent advances in the research of polyanion-type cathode materials for Li-ion batteries. *Energy Environ. Sci.* **2011**, *4*, 3223.

10. Dawei, S.; Guoxiu, W., Single-Crystalline Bilayered V_2O_5 Nanobelts for High-Capacity Sodium-Ion Batteries. *Acs Nano* **2013**, *7*, 11218-11226.

11. Gong, Z.; Yang, Y., The application of synchrotron X-ray techniques to the study of rechargeable batteries. *J. Energy Chem.* **2018**, *27*, 1566-1583.

12. Manthiram, A.; Choi, J., Chemical and structural instabilities of lithium ion battery cathodes. *J. Power Sources* **2006**, *159*, 249-253.

13. Hu, E.; Yu, X.; Lin, R.; Bi, X.; Lu, J.; Bak, S.; Nam, K.-W.; Xin, H. L.; Jaye, C.; Fischer, D. A.; Amine, K.; Yang, X.-Q., Evolution of redox couples in Li- and Mn-rich cathode materials and mitigation of voltage fade by reducing oxygen release. *Nat. Energy* **2018**, *3*, 690-698.

14. Lee, E.; Brown, D. E.; Alp, E. E.; Ren, Y.; Lu, J.; Woo, J.-J.; Johnson, C. S., New Insights into the Performance Degradation of Fe-Based Layered Oxides in Sodium-Ion Batteries: Instability of Fe^{3+}/Fe^{4+} Redox in α-$NaFeO_2$. *Chem. Mater.* **2015**, *27*, 6755-6764.

15. Lin, Z.; Liu, T.; Ai, X.; Liang, C., Aligning academia and industry for unified battery performance metrics. *Nat. Commun.* **2018**, *9*, 5262.

16. Koga, H.; Croguennec, L.; Menetrier, M.; Douhil, K.; Belin, S.; Bourgeois, L.; Suard, E.; Weill, F.; Delmas, C., Reversible Oxygen Participation to the Redox Processes Revealed for $Li_{1.20}Mn_{0.54}Co_{0.13}Ni_{0.13}O_2$. *J. Electrochem. Soc.* **2013**, *160*, A786-A792.

17. Li, X.; Qiao, Y.; Guo, S.; Xu, Z.; Zhu, H.; Zhang, X.; Yuan, Y.; He, P.; Ishida, M.; Zhou, H., Direct Visualization of the Reversible O^{2-}/O^- Redox Process in Li-Rich Cathode Materials. *Adv.*

Mater. **2018**, *30*, 1705197.

18.   Gent, W. E.; Lim, K.; Liang, Y.; Li, Q.; Barnes, T.; Ahn, S. J.; Stone, K. H.; McIntire, M.; Hong, J.; Song, J. H.; Li, Y.; Mehta, A.; Ermon, S.; Tyliszczak, T.; Kilcoyne, D.; Vine, D.; Park, J. H.; Doo, S. K.; Toney, M. F.; Yang, W.; Prendergast, D.; Chueh, W. C., Coupling between oxygen redox and cation migration explains unusual electrochemistry in lithium-rich layered oxides. *Nat. Commun.* **2017**, *8*, 2091.

19.   Sathiya, M.; Rousse, G.; Ramesha, K.; Laisa, C. P.; Vezin, H.; Sougrati, M. T.; Doublet, M. L.; Foix, D.; Gonbeau, D.; Walker, W.; Prakash, A. S.; Ben Hassine, M.; Dupont, L.; Tarascon, J. M., Reversible anionic redox chemistry in high-capacity layered-oxide electrodes. *Nat. Mater.* **2013**, *12*, 827-835.

20.   Song, S.; Kotobuki, M.; Zheng, F.; Xu, C.; Hu, N.; Lu, L.; Wang, Y.; Li, W.-D., Y-Doped Na_2ZrO_3: A Na-Rich Layered Oxide as a High-Capacity Cathode Material for Sodium-Ion Batteries. *ACS Sustainable Chem. Eng.* **2017**, *5*, 4785-4792.

21.   Zhang, X.; Qiao, Y.; Guo, S.; Jiang, K.; Xu, S.; Xu, H.; Wang, P.; He, P.; Zhou, H., Manganese-Based Na-Rich Materials Boost Anionic Redox in High-Performance Layered Cathodes for Sodium-Ion Batteries. *Adv. Mater.* **2019**, *31*, 1807770.

22.   Qiao, Y.; Guo, S.; Zhu, K.; Liu, P.; Li, X.; Jiang, K.; Sun, C.-J.; Chen, M.; Zhou, H., Reversible anionic redox activity in Na_3RuO_4 cathodes: a prototype Na-rich layered oxide. *Energy Environ. Sci.* **2018**, *11*, 299-305.

23.   Otoyama, M.; Jacquet, Q.; Iadecola, A.; Saubanère, M.; Rousse, G.; Tarascon, J.-M., Synthesis and Electrochemical Activity of Some Na(Li)-Rich Ruthenium Oxides with the Feasibility to Stabilize Ru^{6+}. *Adv. Energy Mater.* **2019**, *9*, 1803674.

24. Yang, W.; Devereaux, T. P., Anionic and cationic redox and interfaces in batteries: Advances from soft Xray absorption spectroscopy to resonant inelastic scattering. *J. Power Sources* **2018**, *389*, 188-197.

25. Dai, K.; Wu, J.; Zhuo, Z.; Li, Q.; Sallis, S.; Mao, J.; Ai, G.; Sun, C.; Li, Z.; Gent, W. E.; Chueh, W. C.; Chuang, Y.-d.; Zeng, R.; Shen, Z.-x.; Pan, F.; Yan, S.; Piper, L. F. J.; Hussain, Z.; Liu, G.; Yang, W., High Reversibility of Lattice Oxygen Redox Quantified by Direct Bulk Probes of Both Anionic and Cationic Redox Reactions. *Joule* **2019**, *3*, 518-541.

26. Li, Q.; Qiao, R.; Wray, L. A.; Chen, J.; Zhuo, Z.; Chen, Y.; Yan, S.; Pan, F.; Hussain, Z.; Yang, W., Quantitative probe of the transition metal redox in battery electrodes through soft x-ray absorption spectroscopy. *J. Phys. D: Appl. Phys.* **2016**, *49*, 413003.

27. Mortemard de Boisse, B.; Liu, G.; Ma, J.; Nishimura, S.; Chung, S. C.; Kiuchi, H.; Harada, Y.; Kikkawa, J.; Kobayashi, Y.; Okubo, M.; Yamada, A., Intermediate honeycomb ordering to trigger oxygen redox chemistry in layered battery electrode. *Nat. Commun.* **2016**, *7*, 11397.

28. Manoharan, S. S.; Sahu, R. K., Evidence for an anomalous redox ionic pair between Ru and Mn in $SrRu_{0.5}Mn_{0.5}O_3$: An X-ray absorption spectroscopy approach. *Chem. Commun.* **2002**, *8*, 3068-3069.

29. Mamchik, A.; Dmowski, W.; Egami, T.; Chen, I. W., Magnetic impurities in conducting oxides. II. $(Sr_{1-x}La_x)(Ru_{1-x}Co_x)O_3$ system. *Phys. Rev. B* **2004**, *70*, 104410.

30. Zhuo, Z.; Pemmaraju, C. D.; Vinson, J.; Jia, C.; Moritz, B.; Lee, I.; Sallies, S.; Li, Q.; Wu, J.; Dai, K.; Chuang, Y. D.; Hussain, Z.; Pan, F.; Devereaux, T. P.; Yang, W., Spectroscopic Signature of Oxidized Oxygen States in Peroxides. *J Phys Chem Lett* **2018**, *9*, 6378-6384.

31. Pchelkina, Z. V.; Pitman, A. L.; Moewes, A.; Kurmaev, E. Z.; Tan, T.-Y.; Peets, D. C.; Park, J.-

G.; Streltsov, S. V., Electronic structure of Li_2RuO_3 studied by LDA and LDA+DMFT calculations and soft x-ray spectroscopy. *Phys. Rev. B* **2015**, *91*, 115138.

32. Han, S. W.; Ling, D. C.; Tsai, H. M.; Chuang, C. H.; Wu, S. L.; Pong, W. F.; Chiou, J. W.; Tsai, M. H.; Jang, L. Y.; Lin, H. J.; Pi, T. W.; Lee, J. F., Electronic structure of $RuSr_2EuCu_2O_8$ studied by x-ray absorption and photoemission spectroscopies. *Phys. Rev. B* **2012**, *85*, 014506.

33. Oishi, M.; Fujimoto, T.; Takanashi, Y.; Orikasa, Y.; Kawamura, A.; Ina, T.; Yamashige, H.; Takamatsu, D.; Sato, K.; Murayama, H.; Tanida, H.; Arai, H.; Ishii, H.; Yogi, C.; Watanabe, I.; Ohta, T.; Mineshige, A.; Uchimoto, Y.; Ogumi, Z., Charge compensation mechanisms in $Li_{1.16}Ni_{0.15}Co_{0.19}Mn_{0.50}O_2$ positive electrode material for Li-ion batteries analyzed by a combination of hard and soft X-ray absorption near edge structure. *J. Power Sources* **2013**, *222*, 45-51.

34. Jacquet, Q.; Iadecola, A.; Saubanere, M.; Li, H.; Berg, E. J.; Rousse, G.; Cabana, J.; Doublet, M. L.; Tarascon, J. M., Charge Transfer Band Gap as an Indicator of Hysteresis in LiDisordered Rock Salt Cathodes for Li-Ion Batteries. *J. Am. Chem. Soc.* **2019**, *141*, 11452-11464.

35. Bak, S.-M.; Qiao, R.; Yang, W.; Lee, S.; Yu, X.; Anasori, B.; Lee, H.; Gogotsi, Y.; Yang, X.-Q., Na-Ion Intercalation and Charge Storage Mechanism in 2D Vanadium Carbide. *Adv. Energy Mater.* **2017**, *7*, 1700959.

36. Zhang, L.; Wei, Q.; Sun, D.; Li, N.; Ju, H.; Feng, J.; Zhu, J.; Mai, L.; Cairns, E. J.; Guo, J., Conversion reaction of vanadium sulfide electrode in the lithium-ion cell: Reversible or not reversible? *Nano Energy* **2018**, *51*, 391-399.

37. Ma, C.; Alvarado, J.; Xu, J.; Clement, R. J.; Kodur, M.; Tong, W.; Grey, C. P.; Meng, Y. S., Exploring Oxygen Activity in the High Energy P2-Type $Na_{0.78}Ni_{0.23}Mn_{0.69}O_2$ Cathode Material for Na-Ion Batteries. *J. Am. Chem. Soc.* **2017**, *139*, 4835-4845.

38. Xu, J.; Sun, M.; Qiao, R.; Renfrew, S. E.; Ma, L.; Wu, T.; Hwang, S.; Nordlund, D.; Su, D.; Amine, K.; Lu, J.; McCloskey, B. D.; Yang, W.; Tong, W., Elucidating anionic oxygen activity in lithium-rich layered oxides. *Nat. Commun.* **2018**, *9*, 947.

39. Wu, J.; Li, Q.; Sallis, S.; Zhuo, Z.; Gent, W. E.; Chueh, W. C.; Yan, S.; Chuang, Y.-d.; Yang, W., Fingerprint Oxygen Redox Reactions in Batteries through High-Efficiency Mapping of Resonant Inelastic X-ray Scattering. *Condens. Matter* **2019**, *4*, 5.

40. Igarashi, J.-i.; Nagao, T., Resonant inelastic X-ray scattering spectra at the Ir L-edge in Na_2IrO_3. *J. Electron. Spectrosc. Relat. Phenom.* **2016**, *212*, 44-49.

41. Devereaux, T. P.; Hackl, R., Inelastic light scattering from correlated electrons. *Rev. Mod. Phys.* **2007**, *79*, 175-233.

42. Hong, J.; Gent, W. E.; Xiao, P.; Lim, K.; Seo, D. H.; Wu, J.; Csernica, P. M.; Takacs, C. J.; Nordlund, D.; Sun, C. J.; Stone, K. H.; Passarello, D.; Yang, W.; Prendergast, D.; Ceder, G.; Toney, M. F.; Chueh, W. C., Metal–oxygen decoordination stabilizes anion redox in Li-rich oxides. *Nat. Mater.* **2019**, *18*, 256-265.

43. Perez, A. J.; Jacquet, Q.; Batuk, D.; Iadecola, A.; Saubanère, M.; Rousse, G.; Larcher, D.; Vezin, H.; Doublet, M.-L.; Tarascon, J.-M., Approaching the limits of cationic and anionic electrochemical activity with the Li-rich layered rocksalt Li_3IrO_4. *Nat. Energy* **2017**, *2*, 954-962.

44. Jacquet, Q.; Perez, A.; Batuk, D.; Van Tendeloo, G.; Rousse, G.; Tarascon, J.-M., The $Li_3Ru_yNb_{1-y}O_4$ ($0 \leq y \leq 1$) System: Structural Diversity and Li Insertion and Extraction Capabilities. *Chem. Mater.* **2017**, *29*, 5331-5343.

45. Seo, D. H.; Lee, J.; Urban, A.; Malik, R.; Kang, S.; Ceder, G., The structural and chemical origin of the oxygen redox activity in layered and cation-disordered Li-excess cathode materials.

Nature Chem. **2016**, *8*, 692-697.

46. Mccalla, E.; Abakumov, A. M.; Saubanère, M.; Foix, D.; Berg, E. J.; Rousse, G.; Doublet, M. L.; Gonbeau, D.; Novák, P.; Van, T. G., Visualization of O-O peroxo-like dimers in high-capacity layered oxides for Li-ion batteries. *Science* **2015**, *350*, 1516-1521.

47. Perez, A. J.; Batuk, D.; Saubanère, M.; Rousse, G.; Foix, D.; McCalla, E.; Berg, E. J.; Dugas, R.; H. W. van den Bos, K.; Doublet, M.-L.; Gonbeau, D.; Abakumov, A. M.; Van Tendeloo, G.; Tarascon, J.-M., Strong Oxygen Participation in the Redox Governing the Structural and Electrochemical Properties of Na-Rich Layered Oxide Na_2IrO_3. *Chem. Mater.* **2016**, *28*, 8278-8288.

48. Saubanère, M.; McCalla, E.; Tarascon, J. M.; Doublet, M. L., The intriguing question of anionic redox in high-energy density cathodes for Li-ion batteries. *Energy Environ. Sci.* **2016**, *9*, 984-991.

49. Wang, K.; Yan, P.; Sui, M., Phase Transition Induced Cracking Plaguing Layered Cathode for Sodium-Ion Battery. *Nano Energy* **2018**, *54*, 148-155.

50. Myeong, S.; Cho, W.; Jin, W.; Hwang, J.; Yoon, M.; Yoo, Y.; Nam, G.; Jang, H.; Han, J. G.; Choi, N. S.; Kim, M. G.; Cho, J., Understanding voltage decay in lithium-excess layered cathode materials through oxygen-centred structural arrangement. *Nat. Commun.* **2018**, *9*, 3285.